



Published in final edited form as:

*Circ Res.* 2017 January 06; 120(1): 39–48. doi:10.1161/CIRCRESAHA.116.309283.

## A Precision Medicine Approach to the Rescue of Function on Malignant Calmodulinopathic Long QT Syndrome

Worawan B. Limpitikul<sup>1</sup>, Ivy E. Dick<sup>1,2</sup>, David J. Tester<sup>3</sup>, Nicole J. Boczek<sup>3</sup>, Pattraranee Limphong<sup>4</sup>, Wanjun Yang<sup>1</sup>, Myoung Hyun Choi<sup>1</sup>, Jennifer Babich<sup>1</sup>, Deborah DiSilvestre<sup>4</sup>, Ronald J. Kanter<sup>5</sup>, Gordon F. Tomaselli<sup>4</sup>, Michael J. Ackerman<sup>3</sup>, and David T. Yue<sup>1</sup>

<sup>1</sup>Calcium Signals Laboratory, Department of Biomedical Engineering, The Johns Hopkins University School of Medicine, Ross Research Building, Room 713, 720 Rutland Avenue, Baltimore, MD 21205

<sup>2</sup>Department of Physiology, The University of Maryland School of Medicine, 660 West Redwood St, Howard Hall, Room 511, Baltimore, MD 21205

<sup>3</sup>Departments of Cardiovascular Diseases (Division of Heart Rhythm Services), Pediatrics (Division of Pediatric Cardiology), and Molecular Pharmacology and Experimental Therapeutics (Windland Smith Rice Sudden Death Genomics Laboratory), Guggenheim 501, Mayo Clinic, Rochester, MN, 55905

<sup>4</sup>Division of Cardiology, Department of Medicine, The Johns Hopkins University School of Medicine, Ross Research Building, Room 844, 720 Rutland Avenue Baltimore, MD 21205

<sup>5</sup>Division of Cardiology, Nicklaus Children's Hospital, Miami, FL, 33155

### Abstract

**Rationale**—Calmodulinopathies comprise a new category of potentially life-threatening genetic arrhythmia syndromes capable of producing severe long QT syndrome (LQTS) with mutations involving either *CALM1*, *CALM2*, or *CALM3*. The underlying basis of this form of LQTS is a disruption of Ca<sup>2+</sup>/CaM-dependent inactivation (CDI) of L-type Ca<sup>2+</sup> channels (LTCCs).

**Objective**—To gain insight into the mechanistic underpinnings of calmodulinopathies and devise new therapeutic strategies for the treatment of this form of LQTS.

**Methods and Results**—We generated and characterized the functional properties of iPSC-derived cardiomyocytes (iPSC-CMs) from a patient with D130G-*CALM2*-mediated LQTS, thus creating a platform with which to devise and test novel therapeutic strategies. The patient-derived iPSC-CMs display (1) significantly prolonged action potentials (APs), (2) disrupted Ca<sup>2+</sup> cycling properties, and (3) diminished CDI of LTCCs. Next, taking advantage of the fact that calmodulinopathy patients harbor a mutation in only one of six redundant CaM-encoding alleles,

---

**Address correspondence to:** Dr. Gordon Tomaselli, Department of Medicine, The Johns Hopkins Univ. School of Medicine, Ross Research Building, Room 844, 720 Rutland Avenue, Baltimore, MD 21205, Tel: 410-955-2774, Fax: 410-502-2096, gtomasel@jhmi.edu, Dr. Michael Ackerman, Departments of Cardiovascular Diseases, Mayo Clinic, Guggenheim 501, Rochester, MN, 55905, Tel: 507-284-0101, Fax: 507-284-3757, ackerman.michael@mayo.edu.

### DISCLOSURES

D.J.T.: Transgenomic (royalties); M.J.A.: Boston Scientific, Gilead Sciences, Medtronic, and St. Jude Medical (consultant), Transgenomic (royalties). The rest of the authors declare no competing financial interests.

we devised a strategy using CRISPR interference (CRISPRi) to selectively suppress the mutant gene while sparing the wild-type counterparts. Indeed, suppression of *CALM2* expression produced a functional rescue in iPSC-CMs with D130G-*CALM2*, as shown by the normalization of AP duration and CDI following treatment. Moreover, CRISPRi can be designed to achieve selective knockdown of any of the three *CALM* genes, making it a generalizable therapeutic strategy for any calmodulinopathy.

**Conclusions**—Overall, this therapeutic strategy holds great promise for calmodulinopathy patients as it represents a generalizable intervention capable of specifically altering CaM expression and potentially attenuating LQTS-triggered cardiac events, thus initiating a path towards precision medicine.

### Keywords

Long-QT syndrome; Calmodulin; L-type calcium channels; Ca<sup>2+</sup>-CaM-dependent inactivation (CDI); induced-pluripotent stem cells (iPSCs)

### Subject Terms

Ion Channels/Membrane Transport; Electrophysiology; Stem Cells; Gene Therapy; Arrhythmias

## INTRODUCTION

An increasingly recognized group of patients suffer from diseases called calmodulinopathies, caused by missense mutations in calmodulin (CaM), a ubiquitous Ca<sup>2+</sup> sensor vital to immune system, heart, and brain function. Calmodulinopathy patients often experience life-threatening cardiac arrhythmias associated with long QT syndrome (LQTS)<sup>1–4</sup>, catecholaminergic polymorphic ventricular tachycardia (CPVT)<sup>3, 5</sup>, and idiopathic ventricular fibrillation (IVF)<sup>6</sup>. Their symptoms are often resistant to conventional therapy, suggesting alternate underlying disease mechanisms which require novel therapeutic strategies.

LQTS-associated CaM mutations are known to alter the Ca<sup>2+</sup>/CaM binding affinity<sup>2</sup>, implicating a myriad of Ca<sup>2+</sup>/CaM binding partners as potential pathogenic elements. The L-type Ca<sup>2+</sup> channel (LTCC), which plays a vital role in LQTS, represents one such target<sup>7–10</sup>. In fact, LQTS-associated calmodulinopathy mutations (D96V, D130G, and F142L) mediate a decrease in Ca<sup>2+</sup>/CaM-dependent inactivation (CDI) of LTCCs, a critical form of channel regulation<sup>8</sup>. This would result in the failure of calmodulinopathy-affected LTCCs to inactivate during the plateau of the cardiac action potential (AP), and is predicted to prolong the AP duration (APD), a cellular correlate of prolonged QT intervals identified on the electrocardiogram<sup>10, 11</sup>.

There are three distinct calmodulin genes, *CALM1* (chr14q31), *CALM2* (chr2p21), and *CALM3* (chr19q13), with 85% nucleotide sequence homology that encode for completely identical 149 amino-acid CaM proteins. In all reported cases of LQTS-associated calmodulinopathies, the mutation occurs heterozygously in one of these three redundant *CALM* genes, i.e. with only one out of six alleles harboring the mutation. Thus, only a small

fraction of mutant CaM protein causes the severe phenotype. This large dominant negative effect may be rationalized by the known pre-association of Ca<sup>2+</sup>-free CaM to the LTCCs<sup>10, 12</sup>. In fact, the reduction of CDI due to mutant CaM expression corresponds to a highly non-linear effect such that a relatively small amount of mutant CaM can significantly decrease CDI in HEK293 cells<sup>10</sup>. However, this phenomenon remains to be substantiated in a cardiac system under conditions mimicking that of a calmodulinopathy patient. To this end, we generated induced pluripotent stem cells (iPSCs) from a patient harboring a heterozygous p.D130G-CaM mutation<sup>1</sup> resulting from a single nucleotide substitution (c. 389 A>G) within the *CALM2* gene. Cardiomyocytes (CMs) differentiated from these cells (iPSC-CMs) offer an ideal platform for exploring the dominant negative effect of mutant CaM within a patient-specific genetic background and provide a model system with which to understand the pathogenesis and treatment options of CaM-mediated LQTS.

The non-linear CDI effect in calmodulinopathies may also provide an opportunity for novel therapeutic interventions. Impaired repolarization resulting from a deficit of LTCC CDI exhibits a non-linear threshold such that the fraction of channels harboring a CDI deficit can increase without overt electrical dysfunction up to a critical threshold. At this point, addition of even a minute fraction of affected channels generates the substrate for flagrant arrhythmogenesis<sup>8</sup>. Should this threshold behavior hold true, a relatively small decrease in mutant CaM could result in a significant increase in electrical stability and thus lead to substantial clinical improvement. To this end, we exploit the precise genetic control of a variant of CRISPR/Cas9 technology, CRISPR interference (CRISPRi)<sup>13–15</sup>, to selectively down-regulate mutant CaM expression without permanently altering the genome. Taking advantage of the fact that patients with calmodulinopathies harbor mutations in only one of three *CALM* genes, mutant CaM could be attenuated while largely sparing wild-type CaM. As a test bed for therapeutic development, we utilize our D130G-CaM containing iPSC-CMs (iPSC<sub>D130G-CaM</sub>-CMs), as these cells are able to form a functional syncytium with the genetic background of the patient. Such a disease model readily permits application of CRISPRi to down-regulate mutant *CALM* genes and enables analysis of the functional effects of such a manipulation.

In this study, we demonstrate that iPSC-CMs derived from a patient harboring the p.D130G-CaM missense mutation within *CALM2* accurately recapitulate the cellular LQTS phenotype. Specifically, the iPSC<sub>D130G-CaM</sub>-CMs demonstrate prolonged APs, disrupted Ca<sup>2+</sup> cycling, and diminished LTCC CDI, consistently across extended culture time. Having established a viable model system, we next use CRISPRi to selectively silence the expression of the *CALM2* gene (both mutant and wild-type *CALM2* alleles) and correlate this reduction with a functional rescue of the iPSC<sub>D130G-CaM</sub>-CMs. In particular, we have corrected fully the magnitude of CDI in these cells, resulting in normalization of the AP profile and therapeutic attenuation of the APD.

## METHODS

### Study participant

A p.D130G-CaM missense mutation secondary to c.389 A>G-CALM2 was identified previously in a young female patient with severe LQTS that was referred to the Windland

Smith Rice Sudden Death Genomics Laboratory (M.J.A.) at Mayo Clinic, Rochester, MN for research-based genetic testing<sup>1</sup>. This study was approved by the Mayo Foundation Institutional Review Board and informed consent was obtained.

### Generation of iPSCs

Dermal fibroblasts were isolated from a punch skin biopsy obtained from the p.D130G-CaM positive patient and expanded in DMEM containing 10% FBS. These fibroblasts were reprogrammed using the CytoTune-iPS 2.0 Sendai Reprogramming Kit (Invitrogen) according to manufacturer's recommendations. Colonies were isolated as separate clones and characterized for pluripotency based on immunofluorescent staining (Online Figures. I, II). Sanger sequencing of genomic DNA of each clone confirmed a heterozygous mutation c.389 A>G-CALM2. Wild-type iPSCs used for control experiments were a generous gift from Dr. Bruce Conklin<sup>16</sup>. All cell lines were tested negative for mycoplasma.

### Cell culture

iPSCs were cultured and differentiated in a feeder-free and xeno-free system using a modified protocol described previously<sup>17</sup>. Briefly, iPSCs were cultured on Geltrex matrix (Gibco)-coated tissue culture plates and fed daily with Essential 8 medium (Gibco). When cells were ~30% confluent, they were mechanically dissociated using 0.5 mmol/L EDTA in Dulbecco's Phosphate Buffered Saline (DPBS). For differentiation into cardiomyocytes, cells were dissociated and plated on fresh Geltrex matrix-coated plates. When confluent (day 0), media was exchanged with RPMI-1640 (Sigma-Aldrich) supplemented with B-27(-insulin) (Gibco) and 6  $\mu\text{mol/L}$  CHIR99021. Cells were maintained in this media for the first 7 days, with medium exchange every 2 days. On day 3, 5  $\mu\text{mol/L}$  IWR-1 was added. On day 7, media was changed to RPMI-1640 with B-27 supplement (Gibco) and was exchanged every 2 days. Spontaneous contraction of iPSC-CMs was observed by day 12.

12–14 days post-differentiation, sheets of contracting iPSC-CMs were dissociated using 0.05% trypsin-EDTA (Gibco). The isolated cells were pre-plated for 4–8 min on Geltrex-coated tissue culture plates in order to decrease the number of non-cardiac cells, and the non-adherent cells were then plated on Geltrex matrix-coated glass coverslips at  $\sim 2.5 \times 10^4$  cells/cm<sup>2</sup> for electrophysiological studies and  $\sim 3 \times 10^5$  cells/cm<sup>2</sup> on plastic coverslips to create monolayers for imaging.

### CRISPRi construction, transfection, and transduction

The lentiviral transfer vectors containing cDNA for enzymatically dead Cas9 fused with suppressor Krüppel-associated box (KRAB) and blue fluorescence protein (BFP) (pHR-SFFV-dCas9-BFP-KRAB) was purchased from Addgene (Plasmid #46911). BFP was replaced with monomeric ruby red fluorescence protein (mRuby). The entire construct (dCas9-mRuby-KRAB) was then cloned via Gibson assembly (New England Biolabs) into the lentiviral vector pRRLsin18.cPPT.CMV.eGFP.Wpre54<sup>18</sup>. The lentiviral vector (pKLV-U6gRNA(BbsI)-PGKpuro2ABFP) containing cDNA for the gRNA backbone (driven by the human U6 promoter) and a BFP marker (driven by PGK promoter) was purchased from Addgene (Plasmid #50946) and BFP was replaced with cyan fluorescence protein (CFP). E-CRISPR gRNA sequence prediction program<sup>19</sup> was used to generate candidate gRNA

sequences that selectively complement to the human CALM2 gene (Online Table I). The candidate gRNA sequences were then cloned into the aforementioned lentiviral transfer vector using Golden Gate assembly.

For gRNA screening, both dCas9-mRuby-KRAB and candidate gRNA were expressed in HEK293 cells by transfection with polyethylenimine<sup>10</sup>. For iPSC-CM transduction, lentivirus was generated using Lenti-X-Concentrator (Clontech) according to the manufacturer's recommendations and added to monolayers on day 21 post-differentiation. Expression was confirmed by mRuby and CFP visualization.

### MRNA expression

Total RNA was extracted 4 days post-transfection in HEK293 cells and 8-9 days post-transduction in iPSC-CMs using an RNeasy kit (Qiagen). Complementary DNA was made using the high-capacity cDNA reverse transcription kit (Applied Biosystems). Quantification of CALM mRNA levels was performed using real time PCR (qPCR) with TaqMan gene expression assay (Applied Biosystems). CALM expression level was normalized to the expression level of a house-keeping gene glyceraldehyde 3-phosphate dehydrogenase (GAPDH). Probe numbers: CALM1; Hs00300085\_s1, CALM2; Hs00830212\_s1, CALM3; Hs00968732\_g1, and GAPDH; Hs02758991\_g1.

### Electrophysiology

Whole-cell recordings of iPSC-CMs were performed 28-30 days post-differentiation at room temperature using an Axopatch 200B amplifier (Axon Instruments). Traces were lowpass filtered at 2 kHz, and digitally sampled at 10 kHz. P/8 leak subtraction was used, with series resistances of 1-2 MΩ. Internal solutions contained, (in mmol/L): CsMeSO<sub>3</sub>, 114; CsCl, 5; MgCl<sub>2</sub>, 1; MgATP, 4; HEPES (pH 7.3), 10; BAPTA, 10; and ryanodine, 0.005; at 295 mOsm adjusted with CsMeSO<sub>3</sub>. Seals were formed in Tyrode's solution containing (in mmol/L): NaCl, 135; KCl, 5.4; CaCl<sub>2</sub>, 1.8; MgCl<sub>2</sub>, 0.33; NaH<sub>2</sub>PO<sub>4</sub>, 0.33; HEPES, 5; glucose, 5 (pH 7.4). Following patch rupture, bath solution was switched to Ca<sup>2+</sup>- or Ba<sup>2+</sup>- external solution containing (in mmol/L): TEA-MeSO<sub>3</sub>, 140; HEPES (pH 7.4), 10; and CaCl<sub>2</sub> or BaCl<sub>2</sub>, 5 (for 30-day-old iPSC-CMs) or 40 (for 60-day-old iPSC-CMs); at 300 mOsm, adjusted with TEA-MeSO<sub>3</sub>. The extent of CDI after a 50-ms depolarization ( $f_{50}$ ) was calculated as:

$$f_{50} = \left( r_{50/Ba} - r_{50/Ca} \right) / r_{50/Ba} \quad (1)$$

where  $r_{50/Ba}$  and  $r_{50/Ca}$  are currents remaining after 50-ms with Ba<sup>2+</sup>- and Ca<sup>2+</sup>-containing external solution.

### Imaging

Monolayers of iPSC-CMs expressing either a genetically encoded voltage or Ca<sup>2+</sup> sensor (ASAP1<sup>20</sup> or GCaMP6f<sup>21</sup> respectively via lentiviral transduction) were paced using a custom field stimulation apparatus in RPMI-1640 medium with B-27 supplement. Expression efficiency of the genetically encoded sensors was assessed via flow cytometry (Online Figure III). At 30, 45, and 60 days post-differentiation, green fluorescence was

imaged with an Evolve 512delta camera at 190 frames per second and the relative change in fluorescence signal was measured. The time from upstroke to 80% repolarization ( $APD_{80}$ ) was used to index the APD while the magnitude of peak transient, time to peak, and decay time constant were used as metrics for CaTs. All metrics were quantified using custom Matlab (Mathworks) scripts. For all experiments involving treatment with CRISPRi, control cells were recorded on the same day and were from the same culture, minimizing any culture dependent variability of the cells.

### Statistical analysis

All parameters are shown as mean  $\pm$  SEM. Technical and biological replicates are indicated in the figure legend. The D'Agostino & Pearson omnibus normality test was used to confirm a normal distribution prior to application of the statistical test for comparison of means. Data which did not initially correspond to a normal distribution were logarithmically transformed. The F-test was used to compare variances and a two-sided Student's t-test (adjusted for unequal variance where applicable) was used to compare the difference in means across sample groups. Reported p values are from the two-sided Student's t-test. Minimal sample size to ensure adequate power was determined as previously described<sup>22</sup>.

## RESULTS

### Proband identification and generation of mutation-harboring iPSCs

An increasing number of patients are being diagnosed with calmodulinopathies resulting from single heterozygous missense mutations within their *CALM1*, *CALM2*, or *CALM3* genes. Here, we focus on a p.D130G-CaM mutation identified within *CALM2* of a female infant with severe LQTS<sup>1</sup>. The proband was born at term, and noted to have bradycardia (Figure 1). An ECG, recorded 12 hours after birth, revealed a QTc of 740 ms and 2:1 atrioventricular block (Figure 1A). She was treated with beta-blockers, phenytoin, spironolactone, potassium, and placement of a single-chamber pacemaker within the first week of life. At 6-years-old, a single-chamber implantable cardioverter-defibrillator was implanted and beta-blocker therapy was continued. At 11 and 14 years old, she experienced appropriate defibrillator discharges for ventricular fibrillation.

Next-generation whole exome sequencing followed by *CALM1*, *CALM2*, and *CALM3* gene-specific analysis identified a p.D130G-CaM mutation (c.389 A>G, *CALM2*) within the patient (Figure 1B). The mutation maps to an EF-hand within CaM (Figure 1C) and, like other calmodulinopathic mutations, causes a reduction in the Ca<sup>2+</sup> binding affinity<sup>2</sup>. In order to create a model system with which to understand the pathogenesis and treatment options for this type of CaM-mediated LQTS, multiple clones of iPSCs were generated from the patient's skin biopsy. Two clones with normal karyotypes at passage 25 and expressing the pluripotency markers (Nanog, Oct4, and SSEA4) were selected (Online Figure I). In addition, the ability to generate each of the three germ layers was confirmed by staining differentiated embryoid bodies for  $\alpha$ -fetoprotein (endoderm), smooth muscle actin (mesoderm), and glial fibrillary acidic protein (ectoderm) and by analysis of teratoma formation (Online Figure II). Monolayers of iPSC-CMs (iPSC<sub>D130G-CaM</sub>-CMs) were then generated from these two clones of iPSCs.

To confirm that the background of these iPSC<sub>D130G-CaM</sub>-CMs was not significantly different than iPSCs derived from healthy individuals, we quantified the mRNA levels for multiple proteins that could potentially alter cardiac action potential morphology and/or EC coupling. Compared to wild-type iPSC-CMs (iPSC<sub>WT</sub>-CMs), we found no difference in the mRNA levels of *CALM1*, *CALM2*, *CALM3*, *CACNA1C*, *KCNH2*, *NCX1*, *SCN5A*, *PLN* or *SERCA2* (Online Figure IV). Only *KCNQ1* and *RYR2* appeared somewhat elevated in the iPSC<sub>D130G-CaM</sub>-CMs; however, this variation would not be expected to contribute to a LQT phenotype. Importantly, this validates our iPSC<sub>WT</sub>-CMs as a relevant control, despite the potential variability which can occur due to differing genetic backgrounds<sup>23</sup>.

### Altered APs and calcium transients (CaTs) in iPSC<sub>D130G-CaM</sub>-CMs

Previous work has linked mutations in CaM with LQTS; however, direct evidence demonstrating AP prolongation due to the D130G-CaM mutation has yet to be shown in human cardiomyocytes. We therefore characterized the iPSC<sub>D130G-CaM</sub>-CMs in order to confirm that these cells exhibit prolonged APDs that typically underlie LQTS. To measure APDs, the monolayers were transduced with the genetically encoded voltage sensor ASAP1, which features rapid kinetics and stable long-term expression, allowing accurate APD measurements over multiple time points<sup>20</sup>. The resultant APDs (Figures 1D, E) measured from wild-type iPSC-CMs (iPSC<sub>WT</sub>-CMs) were comparable to those previously reported (Online Table I)<sup>16, 24</sup>. Under these same conditions, iPSC<sub>D130G-CaM</sub>-CMs exhibited dramatically longer APs and APDs (Figures 1G, J; red) as compared to their WT counterparts (gray). This result could be observed at multiple pacing frequencies (Figures 1H, K), a feature associated with increased arrhythmogenic risk<sup>25</sup>. Moreover, the phenotype was stable over long periods of time in culture, such that APDs measured at 30 days in culture were not significantly different than those measured after 45 days or 60 days (Figures 1F, I, L; Online Figure VI).

In addition to the electrical disturbance, dysfunctions in Ca<sup>2+</sup> cycling are often associated with arrhythmogenesis in LQTS<sup>26</sup>. As such, we examined the intracellular Ca<sup>2+</sup> transients (CaTs) of iPSC-CMs using GCaMP6f, a genetically encoded Ca<sup>2+</sup> sensor with a high signal-to-noise ratio and fast kinetics<sup>21</sup>. Figure 2A shows the CaTs from a monolayer of iPSC<sub>WT</sub>-CMs paced at 0.25 Hz with the rise and decay kinetics comparable to those previously reported<sup>27</sup>. However, monolayers of iPSC<sub>D130G-CaM</sub>-CMs exhibit CaT amplitudes over three times larger than WT with slower rise and decay kinetics (Figures 2B–F), akin to the phenotype observed in CaM<sub>D130G</sub>-overexpressing rodent myocytes<sup>10, 11</sup>. Likewise, these CaT effects were stable over time (Online Figure VII). While SR content of the iPSC<sub>D130G-CaM</sub>-CMs was not significantly different from the WT myocytes (Online Figure VIII), the trend was in the direction of increased SR Ca<sup>2+</sup>. Thus, the patient-derived iPSC<sub>D130G-CaM</sub>-CMs recapitulate the LQTS phenotype, demonstrating significant proarrhythmic potential despite limited, native expression levels of CaM<sub>D130G</sub>.

### iPSC<sub>D130G-CaM</sub>-CMs exhibit diminished CDI

Previous studies have implicated the cardiac LTCC as a major contributor to the LQT phenotype in patients with CaM-mediated LQTS<sup>10, 11</sup>. In particular, the D130G mutation weakens the affinity of Ca<sup>2+</sup> binding to CaM<sup>2</sup>, resulting in a significant decrease in CDI

when CaM<sub>D130G</sub> is overexpressed in rodent myocytes<sup>10, 11</sup>. However, the relevance of these results remains to be established in human CMs with physiological levels of mutant CaM expression. We therefore examined the effect of the D130G mutation on LTCC CDI in patient-derived iPSC-CMs. To this end, we performed whole-cell patch clamp recordings of individual CMs. iPSC<sub>WT</sub>-CMs exhibited a rapid decay in their Ca<sup>2+</sup> current in response to a 10-mV depolarizing step (Figure 3A, red). To isolate the extent of pure CDI, Ba<sup>2+</sup>, which binds poorly to CaM, was used as the charge carrier to gauge the extent of voltage-dependent inactivation (VDI) within the same cell<sup>10</sup>. CDI can be seen as the excess inactivation of the Ca<sup>2+</sup> trace (Figure 3A; red), as compared to the Ba<sup>2+</sup> trace (black). Population data showing the average normalized peak Ba<sup>2+</sup> currents as a function of voltage is shown in Figure 3B. For CDI quantification, we first measure the fraction of current remaining after 50 ms (*t*<sub>50</sub>) for both the Ca<sup>2+</sup> and Ba<sup>2+</sup> currents. By plotting the *t*<sub>50</sub> values as a function of voltage, a hallmark U-shaped relationship is observed with Ca<sup>2+</sup> as the charge carrier (Figure 3C, red). The difference between the Ba<sup>2+</sup> and Ca<sup>2+</sup> *t*<sub>50</sub> values at 10 mV, normalized by the Ba<sup>2+</sup> *t*<sub>50</sub> value, quantifies the extent of pure CDI (Figure 3C). Applying this same protocol to the iPSC<sub>D130G-CaM</sub>-CMs reveals a profound attenuation in the kinetics and extent of CDI (Figures 3D, G) without altering the voltage activation profile (Figures 3E, H). Quantifying this result across voltages (Figures 3F, I) confirms a significant decrease in CDI (red, *p*<0.01), an effect which is maintained over time in culture (Online Figure IX). Importantly, this reduction of CDI is significant even in the iPSC<sub>D130G-CaM</sub>-CM background, where the patient's other five *CALM* alleles are WT. Thus, these iPSC<sub>D130G-CaM</sub>-CMs not only provide a viable model system for this LQTS-associated calmodulinopathy, but also suggest that the loss of LTCC CDI is a significant underlying mechanism leading to arrhythmogenesis in these patients.

To further bolster this LTCC centric hypothesis, we examined the effects of other potential CaM targets which might contribute to the LQT phenotype of calmodulinopathy patients. To date, only three genetic forms of LQTS result from mutations within a channel known to be modulated by CaM. LQT1 results from loss of function mutations in *KCNQ1*, LQT3 results from gain-of-function mutations in *SCN5A*, and LQT8 is caused by inactivation altering mutations within *CACNA1C*, somewhat mirroring the LTCC effects described in this study. Of these forms of LQT, only LQT8 approaches the extreme APD prolongation seen in calmodulinopathy patients<sup>28, 29</sup>. To corroborate this in our model system, we mimicked the effect of each LQT mechanism pharmacologically. Consistent with clinical findings, enhancement of the current through the LTCC had a profound effect on APD, while blocking I<sub>Ks</sub> or enhancing Na<sub>v</sub>1.5 produced more modest APD prolongation (Online Figure X). We next utilized a validated model of an adult mammalian cardiomyocyte<sup>8, 30-32</sup> to investigate the fraction of channels harboring a CaM<sub>D130G</sub> required to produce electrical instability via and LTCC CDI specific mechanism *in silico* (Online Figure XI). Indeed, only a small fraction of channels harboring CaM<sub>D130G</sub> was necessary to achieve significant arrhythmogenesis in the model cells. Importantly, the simulation predicted a threshold for the induction of electrical instability precisely matching the expected levels of mutant CaM expression in calmodulinopathy patients based on reported *CALM* gene expression<sup>33</sup>. Such a threshold highlights an important therapeutic principle; namely, only a small reduction in

the expression levels of the mutant CaM may be needed to provide significant clinical benefit to patients.

### Toward a new therapeutic strategy

Having confirmed a major role for LTCC CDI deficits in generating the LQT phenotype in this calmodulinopathy patient, we next considered the implications of this mechanism on a novel therapeutic intervention. As our results predict a significant functional benefit conferred by even a small shift in the expression of mutant versus WT CaM (Online Figure XI), we sought to reduce the fraction of mutant CaM expressed in patients with CaM-mediated LQTS. As all three *CALM* genes encode for identical CaM proteins, we reasoned that we might be able to take advantage of the sequence variation at the nucleotide level. We thus utilized CRISPRi<sup>13–15</sup> to decrease the transcription of the *CALM2* alleles, both the WT and the D130G-containing *CALM2* alleles.

The CRISPRi technology uses a short guide RNA (gRNA) which binds specifically to a target nucleotide sequence. By pairing this gRNA with a nuclease dead Cas9 (dCas9) fused to suppressor Krüppel-associated box (KRAB), selective suppression of the target gene could be achieved. Our first step was therefore to optimize gRNA sequences capable of selectively targeting *CALM2*. Sequence optimization was first done *in silico*<sup>19</sup>, followed by evaluation of the efficiency and specificity of each candidate gRNA in HEK293 cells via qPCR (Online Figure XII, Online Table II). We choose design 21 (Figure 4A) as this gRNA specifically reduced the expression of *CALM2*, without appreciable alteration of either *CALM1* or *CALM3*.

Having identified a potential treatment strategy, we next sought to test this approach within our iPSC<sub>D130G-CaM</sub>-CMs. Monolayers were lentivirally transduced with genes encoding dCas9-mRuby-KRAB and gRNA-CFP, and expression of both constructs was confirmed by visualization of red and blue fluorescence, respectively. Compared to untreated iPSC<sub>D130G-CaM</sub>-CMs, the CRISPRi-treated iPSC<sub>D130G-CaM</sub>-CMs exhibited significantly lower levels of *CALM2* mRNA with unaltered levels of *CALM1* and *CALM3* (Figure 4B) mRNA level with the overall reduction of total amount of CaM protein (Online Figure V). In addition, we probed the effect of treatment on multiple cardiac genes and found no significant change in the mRNA levels of *CACNA1C*, *KCNQ1*, *KCNH2*, *SCN5A*, *RYR2*, *SERCA2*, *NCX1* or *PLN* (Online Figure IV). Having achieved a selective decrease in *CALM2* transcription, we next tested if this reduction correlated with a functional effect within the iPSC<sub>D130G-CaM</sub>-CMs. Indeed, treatment of the monolayers resulted in a substantial shortening of the APDs in response to 0.5-Hz stimulation (Figure 4C, blue) as compared to untreated monolayers (gray). This effect was consistent across multiple trials, resulting in a significant decrease in APD as compared to untreated iPSC<sub>D130G-CaM</sub>-CMs (Figure 4C, right), establishing CRISPRi as a robust and promising strategy for the treatment of CaM-mediated LQTS.

Having established functional rescue of the iPSC<sub>D130G-CaM</sub>-CM monolayers, we next considered the underlying mechanism. Our previous results suggest that APD prolongation of these cells stems from a CDI deficit of the LTCC (Figure 3). We therefore predicted that successful treatment of these cells should correspond to a correction (increase) in the CDI of

the LTCCs. Indeed, treated iPSC<sub>D130G-CaM</sub>-CMs displayed significantly faster CDI (Figure 4D) as compared to untreated cells. In fact, CDI in the treated cells was nearly identical to that of iPSC<sub>WT</sub>-CMs (Figure 3). Thus, CRISPRi effectively reduced the expression of the mutant and WT *CALM2* alleles, resulting in normalization of the APD, and restoration of LTCC's CDI mechanism.

### Generalization of the CRISPRi strategy across calmodulinopathy subtypes

Beyond the proband described in this study, the CRISPRi treatment strategy is readily generalizable to any calmodulinopathy. In contrast to the classic CRISPR/Cas9 genome editing technique where the gRNA sequence is tailored to an exact locus within the affected gene, CRISPRi targets the entire gene of interest itself, resulting in repression regardless of the specific base-pair alteration. This technique can therefore be adjusted to target *CALM1* or *CALM3* genes, providing efficacy across calmodulinopathy patient populations agnostic to the phenotype. We thus created gRNA sequences targeting each of the *CALM* genes (Figure 5A, Online Figure XII, Online Table II) and tested their efficacy in iPSC-CMs. Utilizing iPSC<sub>WT</sub>-CMs, we are indeed able to specifically decrease the expression of either *CALM1* (Figure 5B) or *CALM3* (Figure 5C), thus providing a modular toolkit for the treatment of calmodulinopathies resulting from a mutation within any of the three *CALM* genes.

## DISCUSSION

iPSC<sub>D130G-CaM</sub>-CMs provide a good model system for investigating the underlying pathology of LQTS-associated calmodulinopathies. Two distinct iPSC<sub>D130G-CaM</sub>-CM clones each formed a stable contracting syncytium and exhibited prolonged APs, Ca<sup>2+</sup> cycling disturbances, and diminished LTCC CDI across extended culture. Creation of this model system enabled the generation and testing of a new therapeutic strategy. Taking advantage of the genome targeting precision of CRISPRi, we were able to selectively and efficiently silence both the WT and the D130G-containing *CALM2* alleles, resulting in functional rescue of both LTCC CDI and cardiac AP morphology. This proof-of-principle therapy thus represents a first step towards a novel, targeted therapeutic design for calmodulinopathies.

Previous studies on the underlying mechanism of LQTS-associated calmodulinopathies have involved the overexpression of mutant CaM in rodent myocytes<sup>10, 11</sup>. While such studies have implicated the LTCC<sup>10</sup> and ruled out the Na<sub>v</sub>1.5 channel<sup>11</sup> as major contributors to the LQT phenotype of calmodulinopathy patients, they do not represent the native expression levels of mutant CaM. In particular, calmodulinopathy patients harbor a single heterozygous mutation in only one of three redundant *CALM* genes. The ability of the resultant small fraction of mutant CaM protein to produce the severe phenotype seen in patients has been attributed to CaM's pre-association to the LTCC<sup>10</sup>. In this context, a fraction of LTCCs pre-bound to mutant CaM will display diminished CDI, disrupting the precise tuning of the AP by Ca<sup>2+</sup> influx. The profound prolongation of the APs and decreased CDI observed in the iPSC<sub>D130G-CaM</sub>-CMs corroborate just such a dominant negative effect. Moreover, the amelioration of the LQTS phenotype of the iPSC<sub>D130G-CaM</sub>-CMs via suppression of *CALM2* transcription firmly establishes this mutation as the causative genetic mechanism.

However, this new mechanistic insight also presents a significant challenge to the treatment of these calmodulinopathy patients. The pre-association of LTCCs with both mutant and WT CaM makes selective targeting of the disrupted LTCCs nearly impossible. Thus, any treatment option for these patients must selectively target the mutant CaM, prior to cytosolic expression and binding to the LTCC.

Fortunately, CRISPRi provides just such a therapeutic option. In fact, recent work demonstrates that CRISPRi is capable of robust gene knock down within both iPSCs as well as iPSC-derived cardiomyocytes, making this a highly attractive method which has already been validated for our model system. Moreover, this technique offers the advantages of selectivity, reversibility, and generalizability<sup>13–15</sup>. That is, RNA transcription of specific mutation-containing *CALM* genes can be repressed, without modifying the patient genome and risking permanent alteration of off-target or downstream elements<sup>13, 14</sup>. Further, this technique is generalizable to any calmodulinopathy. Here, we present a simple therapeutic toolbox in which three gRNAs targeting either *CALM1*, *CALM2*, or *CALM3* can be chosen to match any calmodulinopathy patient. Importantly, this means that while this study focused on the LQTS-associated calmodulinopathies, the therapy developed here should also be effective for the CPVT- and IVF-associated calmodulinopathies. Moreover, as expected due to the widespread distribution of CaM, calmodulinopathy patients also exhibit extra-cardiac phenotypes including seizures and developmental delays<sup>2</sup>. Importantly, the CRISPRi toolkit should be effective on these non-cardiac symptoms, as targeting of the CRISPRi can be adjusted to include any affected organ systems.

More broadly, this therapeutic principle could be applied to the treatment of any disease in which there is a redundancy of the affected gene. Thus, the CRISPRi strategy described here not only represents a promising new treatment option for calmodulinopathy patients, but could provide a generalizable strategy in the treatment of a variety of diseases. Fortunately, development of CRISPR/Cas9 delivery into patients is already well underway<sup>34</sup>, propelling the translation of these findings towards improving patients' health and quality of life and in the case of patients with a LQTS/CPVT/IVF-associated calmodulinopathy, preventing sudden death in the young.

## Supplementary Material

Refer to Web version on PubMed Central for supplementary material.

## Acknowledgments

David T. Yue passed away on December 23, 2014. His mentorship, wisdom, and kindness are greatly missed.

We thank Drs. Zhaohui Ye and Linchao Cheng for help in conducting teratoma formation assay, Dr. Stephen Eacker, for his insight in optimizing the delivery of CRISPR into iPSCs, and Dr. Peter Anderson for assistance with flow cytometry. We also thank Dr. Leslie Tung for providing valuable advice and discussions, and members of the Calcium Signals Lab for ongoing feedback.

## SOURCES OF FUNDING

American Heart Association Predoctoral Fellowship (W.B.L.), R01MH065531 (W.B.L., I.E.D.), The Magic that Matters Fund and The Zegar Family Foundation (D.D., G.F.T.), Mayo Clinic Windland Smith Rice Comprehensive Sudden Cardiac Death Program (M.J.A.)

## Nonstandard Abbreviations and Acronyms

<b>CaM</b>	calmodulin
<b>LQTS</b>	long QT syndrome
<b>CPVT</b>	catecholaminergic polymorphic tachycardia
<b>IVF</b>	idiopathic ventricular fibrillation
<b>LTCC</b>	L-type Ca <sup>2+</sup> channel
<b>CDI</b>	Ca <sup>2+</sup> /calmodulin-dependent inactivation
<b>AP(D)</b>	action potential (duration)
<b>iPSC(-CM)</b>	induced pluripotent stem cell(-derived cardiomyocyte)
<b>CRISPRi</b>	CRISPR interference
<b>CaT</b>	Ca <sup>2+</sup> transients
<b>VDI</b>	voltage-dependent inactivation
<b>gRNA</b>	guide RNA

## REFERENCES

1. Boczek NJ, Gomez-Hurtado N, Ye D, Calvert ML, Tester DJ, Kryshtal D, Hwang HS, Johnson CN, Chazin WJ, Loporcaro CG, Shah M, Papez AL, Lau YR, Kanter R, Knollmann BC, Ackerman MJ. Spectrum and prevalence of calm1-, calm2-, and calm3-encoded calmodulin (cam) variants in long qt syndrome (lqts) and functional characterization of a novel lqts-associated cam missense variant, e141g. *Circ. Cardiovasc. Genet.* 2016
2. Crotti L, Johnson CN, Graf E, De Ferrari GM, Cuneo BF, Ovadia M, Papagiannis J, Feldkamp MD, Rathi SG, Kunic JD, Pedrazzini M, Wieland T, Lichtner P, Beckmann BM, Clark T, Shaffer C, Benson DW, Kaab S, Meitinger T, Strom TM, Chazin WJ, Schwartz PJ, George AL Jr. Calmodulin mutations associated with recurrent cardiac arrest in infants. *Circulation.* 2013; 127:1009–1017. [PubMed: 23388215]
3. Makita N, Yagihara N, Crotti L, Johnson CN, Beckmann BM, Roh MS, Shigemizu D, Lichtner P, Ishikawa T, Aiba T, Homfray T, Behr ER, Klug D, Denjoy I, Mastantuono E, Theisen D, Tsunoda T, Satake W, Toda T, Nakagawa H, Tsuji Y, Tsuchiya T, Yamamoto H, Miyamoto Y, Endo N, Kimura A, Ozaki K, Motomura H, Suda K, Tanaka T, Schwartz PJ, Meitinger T, Kaab S, Guicheney P, Shimizu W, Bhuiyan ZA, Watanabe H, Chazin WJ, George AL Jr. Novel calmodulin mutations associated with congenital arrhythmia susceptibility. *Circ. Cardiovasc. Genet.* 2014; 7:466–474. [PubMed: 24917665]
4. Reed GJ, Boczek NJ, Etheridge S, Ackerman MJ. Calm3 mutation associated with long qt syndrome. *Heart Rhythm.* 2014
5. Nyegaard M, Overgaard MT, Sondergaard MT, Vranas M, Behr ER, Hildebrandt LL, Lund J, Hedley PL, Camm AJ, Wettrell G, Fosdal I, Christiansen M, Borglum AD. Mutations in calmodulin cause ventricular tachycardia and sudden cardiac death. *Am. J. Hum. Genet.* 2012; 91:703–712. [PubMed: 23040497]
6. Marsman RF, Barc J, Beekman L, Alders M, Dooijes D, van den Wijngaard A, Ratbi I, Sefiani A, Bhuiyan ZA, Wilde AA, Bezzina CR. A mutation in calm1 encoding calmodulin in familial idiopathic ventricular fibrillation in childhood and adolescence. *J. Am. Coll. Cardiol.* 2013

7. Boczek NJ, Ye D, Jin F, Tester DJ, Huseby A, Bos JM, Johnson AJ, Kanter R, Ackerman MJ. Identification and functional characterization of a novel *ca<sub>v</sub>1c*-mediated cardiac disorder characterized by prolonged qt intervals with hypertrophic cardiomyopathy, congenital heart defects, and sudden cardiac death. *Circ Arrhythm Electrophysiol.* 2015; 8:1122–1132. [PubMed: 26253506]
8. Dick IE, Joshi-Mukherjee R, Yang W, Yue DT. Arrhythmogenesis in timothy syndrome is associated with defects in *ca<sub>v</sub>(2+)*-dependent inactivation. *Nat Commun.* 2016; 7:10370. [PubMed: 26822303]
9. Fukuyama M, Wang Q, Kato K, Ohno S, Ding WG, Toyoda F, Itoh H, Kimura H, Makiyama T, Ito M, Matsuura H, Horie M. Long qt syndrome type 8: Novel *ca<sub>v</sub>1c* mutations causing qt prolongation and variant phenotypes. *Europace.* 2014; 16:1828–1837. [PubMed: 24728418]
10. Limpitikul WB, Dick IE, Joshi-Mukherjee R, Overgaard MT, George AL Jr, Yue DT. Calmodulin mutations associated with long qt syndrome prevent inactivation of cardiac l-type *ca<sub>v</sub>(2+)* currents and promote proarrhythmic behavior in ventricular myocytes. *J. Mol. Cell. Cardiol.* 2014; 74:115–124. [PubMed: 24816216]
11. Yin G, Hassan F, Haroun AR, Murphy LL, Crotti L, Schwartz PJ, George AL, Satin J. Arrhythmogenic calmodulin mutations disrupt intracellular cardiomyocyte *ca<sub>v</sub>2+* regulation by distinct mechanisms. *J Am Heart Assoc.* 2014; 3:e000996. [PubMed: 24958779]
12. Erickson MG, Alseikhan BA, Peterson BZ, Yue DT. Preassociation of calmodulin with voltage-gated *ca<sub>v</sub>(2+)* channels revealed by fret in single living cells. *Neuron.* 2001; 31:973–985. [PubMed: 11580897]
13. Gilbert LA, Larson MH, Morsut L, Liu Z, Brar GA, Torres SE, Stern-Ginossar N, Brandman O, Whitehead EH, Doudna JA, Lim WA, Weissman JS, Qi LS. Crispr-mediated modular rna-guided regulation of transcription in eukaryotes. *Cell.* 2013; 154:442–451. [PubMed: 23849981]
14. Qi LS, Larson MH, Gilbert LA, Doudna JA, Weissman JS, Arkin AP, Lim WA. Repurposing crispr as an rna-guided platform for sequence-specific control of gene expression. *Cell.* 2013; 152:1173–1183. [PubMed: 23452860]
15. Mandegar MA, Huebsch N, Frolov EB, Shin E, Truong A, Olvera MP, Chan AH, Miyaoka Y, Holmes K, Spencer CI, Judge LM, Gordon DE, Eskildsen TV, Villalta JE, Horlbeck MA, Gilbert LA, Krogan NJ, Sheikh SP, Weissman JS, Qi LS, So PL, Conklin BR. Crispr interference efficiently induces specific and reversible gene silencing in human ipscs. *Cell stem cell.* 2016
16. Spencer CI, Baba S, Nakamura K, Hua EA, Sears MA, Fu CC, Zhang J, Balijepalli S, Tomoda K, Hayashi Y, Lizarraga P, Wojciak J, Scheinman MM, Aalto-Setälä K, Makielski JC, January CT, Healy KE, Kamp TJ, Yamanaka S, Conklin BR. Calcium transients closely reflect prolonged action potentials in ipsc models of inherited cardiac arrhythmia. *Stem Cell Reports.* 2014; 3:269–281. [PubMed: 25254341]
17. Nakahama H, Di Pasquale E. Generation of cardiomyocytes from pluripotent stem cells. *Methods Mol. Biol.* 2016; 1353:181–190. [PubMed: 25523811]
18. Kapoor A, Sekar RB, Hansen NF, Fox-Talbot K, Morley M, Pihur V, Chatterjee S, Brandimarto J, Moravec CS, Pulit SL, Consortium QTI-IG, Pfeufer A, Mullikin J, Ross M, Green ED, Bentley D, Newton-Cheh C, Boerwinkle E, Tomaselli GF, Cappola TP, Arking DE, Halushka MK, Chakravarti A. An enhancer polymorphism at the cardiomyocyte intercalated disc protein *nos1ap* locus is a major regulator of the qt interval. *Am. J. Hum. Genet.* 2014; 94:854–869. [PubMed: 24857694]
19. Heigwer F, Kerr G, Boutros M. E-crispr: Fast crispr target site identification. *Nat Methods.* 2014; 11:122–123. [PubMed: 24481216]
20. St-Pierre F, Marshall JD, Yang Y, Gong Y, Schnitzer MJ, Lin MZ. High-fidelity optical reporting of neuronal electrical activity with an ultrafast fluorescent voltage sensor. *Nat. Neurosci.* 2014; 17:884–889. [PubMed: 24755780]
21. Chen TW, Wardill TJ, Sun Y, Pulver SR, Renninger SL, Baohan A, Schreiter ER, Kerr RA, Orger MB, Jayaraman V, Looger LL, Svoboda K, Kim DS. Ultrasensitive fluorescent proteins for imaging neuronal activity. *Nature.* 2013; 499:295–300. [PubMed: 23868258]
22. Parker RA, Berman NG. Sample size. *The American Statistician.* 2003; 57:166–170.
23. Sharma A, Wu JC, Wu SM. Induced pluripotent stem cell-derived cardiomyocytes for cardiovascular disease modeling and drug screening. *Stem Cell. Res. Ther.* 2013; 4:150. [PubMed: 24476344]

24. Ma J, Guo L, Fiene SJ, Anson BD, Thomson JA, Kamp TJ, Kolaja KL, Swanson BJ, January CT. High purity human-induced pluripotent stem cell-derived cardiomyocytes: Electrophysiological properties of action potentials and ionic currents. *Am. J. Physiol. Heart Circ. Physiol.* 2011; 301:H2006–H2017. [PubMed: 21890694]
25. Marban E. Cardiac channelopathies. *Nature.* 2002; 415:213–218. [PubMed: 11805845]
26. Xie LH, Weiss JN. Arrhythmogenic consequences of intracellular calcium waves. *Am. J. Physiol. Heart Circ. Physiol.* 2009; 297:H997–H1002. [PubMed: 19561309]
27. Hwang HS, Kryshtal DO, Feaster TK, Sanchez-Freire V, Zhang J, Kamp TJ, Hong CC, Wu JC, Knollmann BC. Comparable calcium handling of human ipsc-derived cardiomyocytes generated by multiple laboratories. *J. Mol. Cell. Cardiol.* 2015; 85:79–88. [PubMed: 25982839]
28. Splawski I, Timothy KW, Decher N, Kumar P, Sachse FB, Beggs AH, Sanguinetti MC, Keating MT. Severe arrhythmia disorder caused by cardiac l-type calcium channel mutations. *Proc. Natl. Acad. Sci. U.S.A.* 2005; 102:8089–8096. discussion 8086-8088. [PubMed: 15863612]
29. Splawski I, Timothy KW, Sharpe LM, Decher N, Kumar P, Bloise R, Napolitano C, Schwartz PJ, Joseph RM, Condouris K, Tager-Flusberg H, Priori SG, Sanguinetti MC, Keating MT. Ca(v)1.2 calcium channel dysfunction causes a multisystem disorder including arrhythmia and autism. *Cell.* 2004; 119:19–31. [PubMed: 15454078]
30. Livshitz LM, Rudy Y. Regulation of ca<sup>2+</sup> and electrical alternans in cardiac myocytes: Role of camkii and repolarizing currents. *Am. J. Physiol. Heart Circ. Physiol.* 2007; 292:H2854–H2866. [PubMed: 17277017]
31. Luo CH, Rudy Y. A dynamic model of the cardiac ventricular action potential. I. Simulations of ionic currents and concentration changes. *Circ. Res.* 1994; 74:1071–1096. [PubMed: 7514509]
32. Luo CH, Rudy Y. A dynamic model of the cardiac ventricular action potential. II. Afterdepolarizations, triggered activity, and potentiation. *Circ. Res.* 1994; 74:1097–1113. [PubMed: 7514510]
33. Petryszak R, Burdett T, Fiorelli B, Fonseca NA, Gonzalez-Porta M, Hastings E, Huber W, Jupp S, Keays M, Kryvych N, McMurry J, Marioni JC, Malone J, Megy K, Rustici G, Tang AY, Taubert J, Williams E, Mannion O, Parkinson HE, Brazma A. Expression atlas update--a database of gene and transcript expression from microarray- and sequencing-based functional genomics experiments. *Nucleic Acids Res.* 2014; 42:D926–D932. [PubMed: 24304889]
34. Ran FA, Cong L, Yan WX, Scott DA, Gootenberg JS, Kriz AJ, Zetsche B, Shalem O, Wu X, Makarova KS, Koonin EV, Sharp PA, Zhang F. In vivo genome editing using staphylococcus aureus cas9. *Nature.* 2015; 520:186–191. [PubMed: 25830891]

## Novelty and Significance

### What Is Known?

- Calmodulinopathies comprise a new category of life-threatening genetic cardiac arrhythmias caused by single heterozygous point mutations within the calcium sensor calmodulin (CaM).
- Calmodulinopathy mutations alter the Ca<sup>2+</sup> binding affinity of CaM, implicating numerous Ca<sup>2+</sup>/CaM binding partners as potential pathogenic elements, including the L-type Ca<sup>2+</sup> channel (LTCC), which exhibits disrupted feedback regulation in the presence of mutant CaM when studied in a heterologous expression system.

### What New Information Does This Article Contribute?

- This study develops a robust model system using induced pluripotent stem cells (iPSCs) derived from a calmodulinopathy patient, which recapitulates the phenotype of the patients and provides a test bed for mechanistic understanding and therapeutic design.
- A mechanistic link between defective Ca<sup>2+</sup> regulation of LTCC and the calmodulinopathy phenotype is established.
- A therapeutic strategy based on CRISPR interference (CRISPRi) demonstrates restoration of the action potential in the calmodulinopathy iPSC cardiomyocytes (iPSC-CMs).

Calmodulinopathies represent a growing class of severe cardiac arrhythmias, which are often resistant to conventional treatments. This disorder is associated with mutations that disrupt Ca<sup>2+</sup> binding to CaM, a ubiquitous Ca<sup>2+</sup> sensor molecule vital to heart and skeletal muscle contraction, memory, and immunological responses. Here, we utilize iPSC-CMs derived from a recently identified calmodulinopathy patient with severe long QT syndrome (LQTS) to create a model system suitable for examining calmodulinopathy pathogenesis and designing therapeutic interventions. Using this model system, we demonstrate a significant impact of the calmodulinopathy mutations on the Ca<sup>2+</sup> regulation of LTCCs, establishing this channel as a major causative factor of the LQTS phenotype. Further, application of CRISPRi robustly suppresses the expression of the mutant CaM gene, and produces a functional rescue of the calmodulinopathy phenotype, as evidenced by the restoration of the cardiac action potential morphology and LTCC function. This therapeutic strategy is generalizable to any calmodulinopathy mutation, thus it holds great promise for improving the health and quality of life of many calmodulinopathy patients

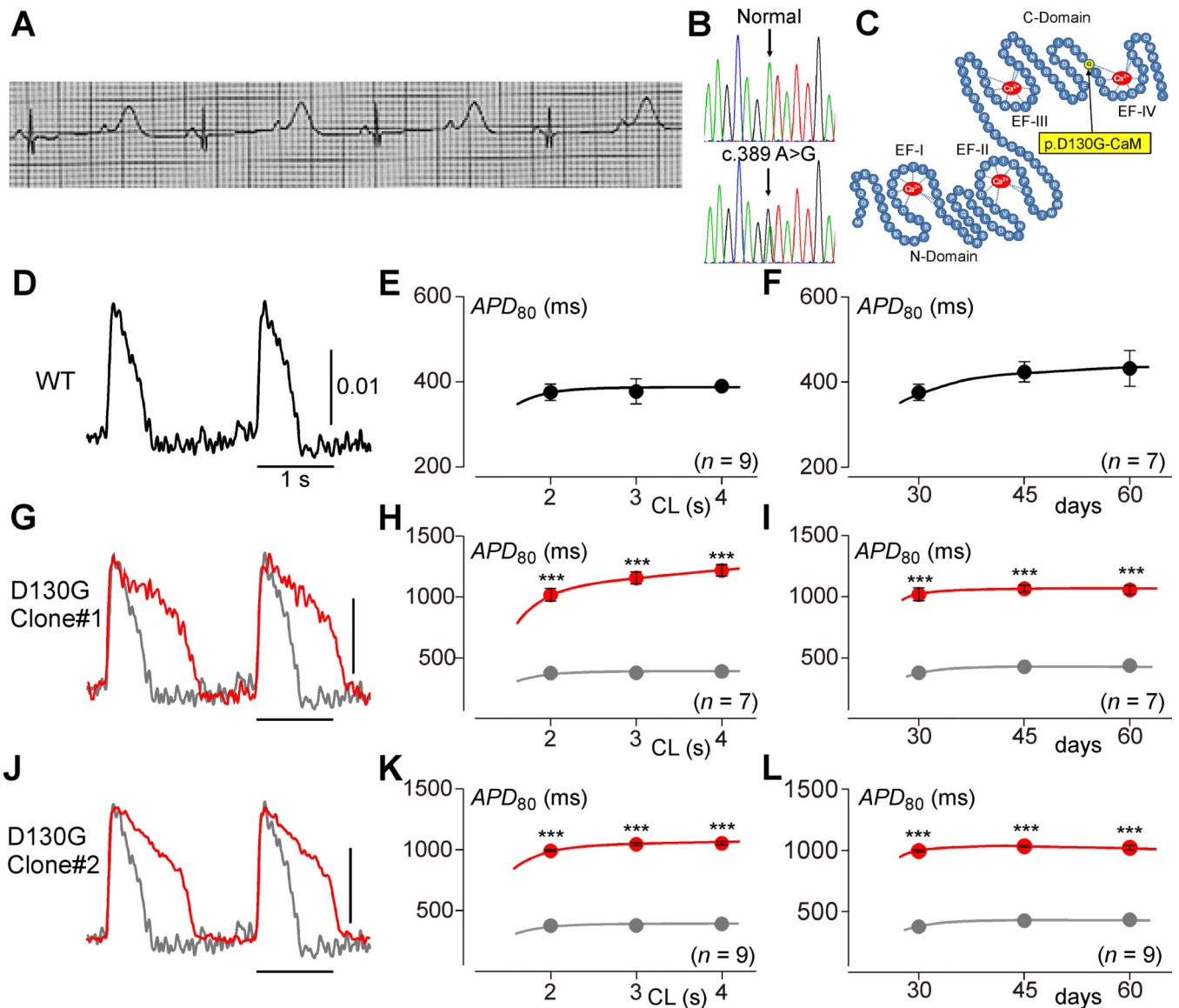


### Figure 1. IPSCs recapitulate the calmodulinopathy phenotype

**A**, The proband's electrocardiogram taken at 12 hours after birth, illustrating a  $\text{QTc} > 700$  ms.

**B**, DNA Sanger sequencing chromatograms for both a normal control (top) and the patient (bottom) revealing a heterozygous c.389 A>G single nucleotide substitution in *CALM2*

resulting in the p.D130G-CaM amino acid substitution. **C**, Schematic rendering of the CaM protein (blue) highlighting the N-domain and C-domain, each containing two EF hands (labeled EF-I through EF-IV) with  $\text{Ca}^{2+}$  (red) bound. Yellow circle indicates the D130G mutation identified in the LQTS patient.

**D**, Exemplar APs from iPSC<sub>WT</sub>-CMs (WT) paced at 0.5 Hz, recorded via fluorescence imaging using ASAP1. Scale bar indicates change in fluorescence as measured by  $F/F_0$ .

**E**, Population data for mean APDs at various pacing cycle lengths (CL) for iPSC<sub>WT</sub>-CMs (n=9). Error bars indicate  $\pm$ SEM throughout. Each biological replicate (n) is an average value of 2 technical replicates, here and throughout this figure.

**F**, Population data for iPSC<sub>WT</sub>-CM APDs at a 2-second cycle length across multiple

time points (n=9, 9, and 7 on day 30, 45, and 60, respectively). **G**, Exemplar APs from iPSC<sub>D130G-CaM</sub>-CMs (red). WT reproduced in gray. **H**, Average APD data for iPSC<sub>D130G-CaM</sub>-CMs (red) (n=7). WT reproduced in gray (\*\*\*) p<0.001 compared to WT; corrected for unequal variance of normal distributions). **I**, Average APDs at a 2-second cycle length from D130G iPSCs are stable across time (n=7, 7, and 7 on day 30, 45, and 60, respectively). **J–L**, Alternate D130G clone demonstrating the same result as **G–I** (n=9, \*\*\* p<0.001 compared to WT and corrected for unequal variance of normal distributions).

Author Manuscript

Author Manuscript

Author Manuscript

Author Manuscript

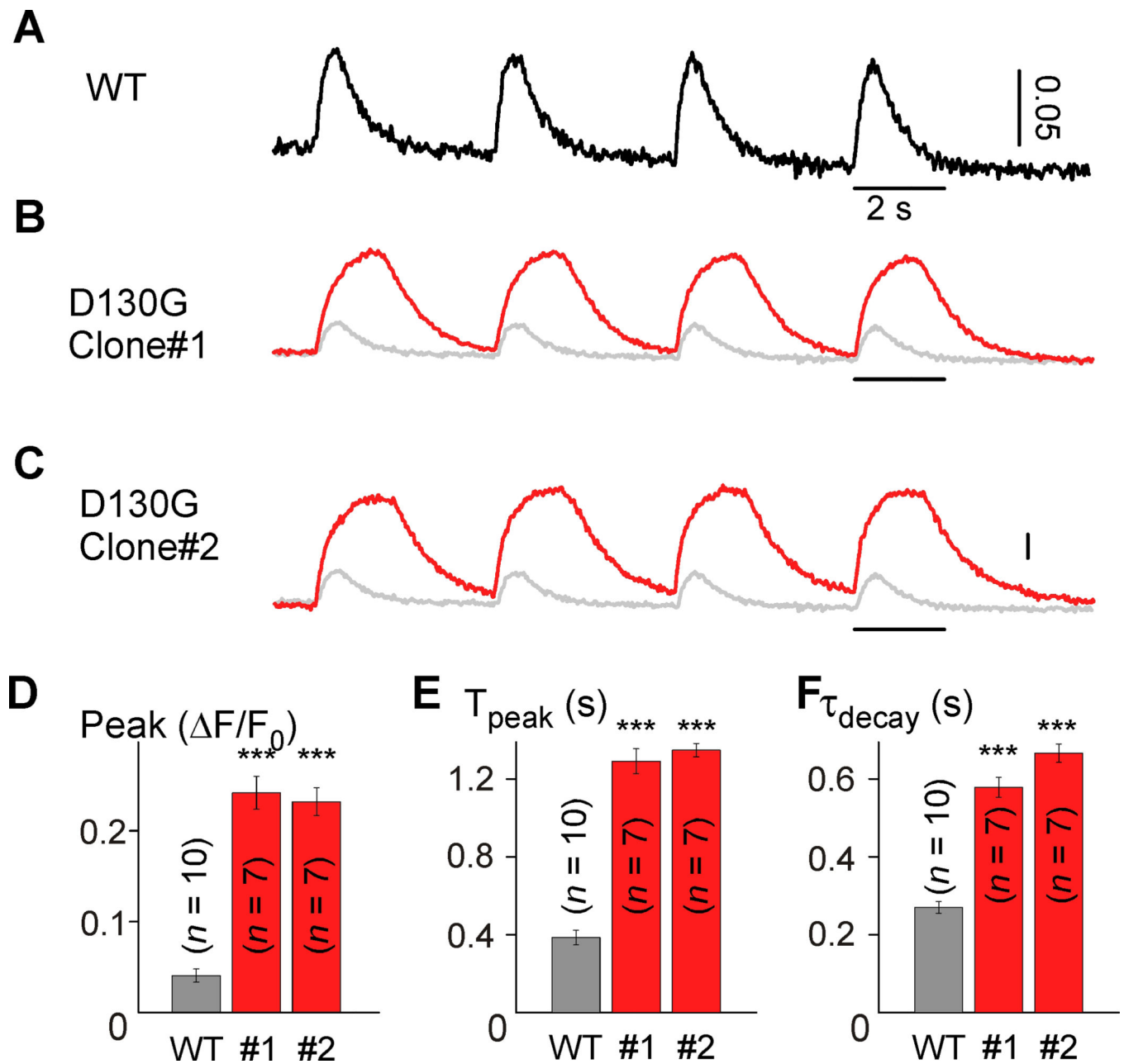


**Figure 2. Disruption of calcium handling in calmodulinopathy iPSCs**

**A**, Exemplar CaTs recorded from iPSC<sub>WT</sub>-CMs (WT) using GCaMP6f. Scale bar indicates change in fluorescence as measured by  $\Delta F/F_0$ . **B**, Exemplar CaTs recorded from iPSC<sub>D130G-CaM</sub>-CMs (red) as compared to WT (gray). **C**, Exemplar CaTs from an alternate D130G clone. **D–F**, Population data demonstrating larger amplitude and slower kinetics for both iPSC<sub>D130G-CaM</sub>-CMs clones (red) (Peak, mean peak fluorescence change;  $T_{\text{peak}}$ , mean time to peak;  $\tau_{\text{decay}}$ , mean decay time constant; \*\*\*  $p < 0.001$  compared to WT and corrected for unequal variance, all populations were normally distributed). Error bars indicate  $\pm$  SEM throughout. Biological replicates (n) are 10, 7, and 7 for WT, D130G clone #1, D130G

clone#2, respectively. Each biological replicate (n) is an average value of 2 technical replicates.

Author Manuscript

Author Manuscript

Author Manuscript

Author Manuscript

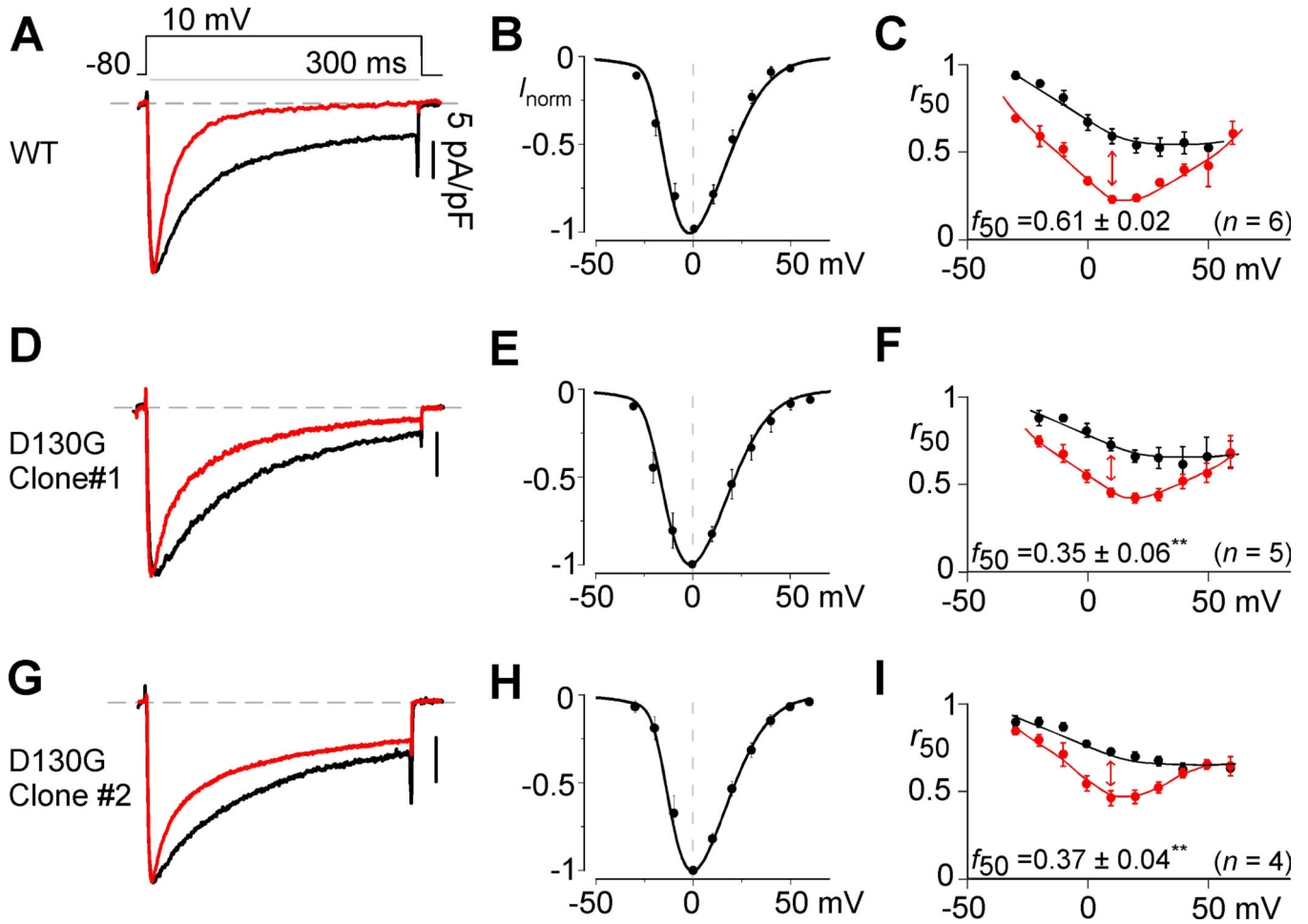


### Figure 3. CDI deficits in calmodulinopathy iPSCs

**A**, Exemplar whole-cell current recordings in  $\text{Ca}^{2+}$  (red) and  $\text{Ba}^{2+}$  (black) for  $\text{iPSC}_{\text{WT}}$ -CMs.  $\text{Ba}^{2+}$  current is normalized to  $\text{Ca}^{2+}$  peak, scale bar corresponds to  $\text{Ca}^{2+}$  here and throughout.

**B**, Mean normalized current and voltage relationship obtained in  $\text{Ba}^{2+}$  for  $\text{iPSC}_{\text{WT}}$ -CMs.

Error bars indicate  $\pm$  SEM throughout. **C**, Population data for  $\text{Ca}^{2+}$  (red) and  $\text{Ba}^{2+}$  (black) for  $\text{iPSC}_{\text{WT}}$ -CMs, where  $r_{50}$  quantifies the extent of current inactivation across voltages. Red arrow depicts extent of CDI ( $f_{50}$ ) at 10-mV test potential here and throughout ( $n=6$  separate cells for **B–C**).

**D**, Exemplar whole-cell current recordings in  $\text{Ca}^{2+}$  (red) and  $\text{Ba}^{2+}$  (black) for  $\text{iPSC}_{\text{D130G-CaM}}$ -CMs ( $n=5$ ).

**E**, There is no significant shift ( $p>0.05$  compared to WT) in the current voltage relationship for  $\text{iPSC}_{\text{D130G-CaM}}$ -CMs as compared to WT **B**.

**F**, Population data demonstrates a significant decrease in CDI for the  $\text{iPSC}_{\text{D130G-CaM}}$ -CMs (\*\* $p<0.01$  compared to WT, corrected for unequal variance).

**G–I**, Alternate D130G clone ( $n=4$ ) demonstrating the same result as **D–F**.

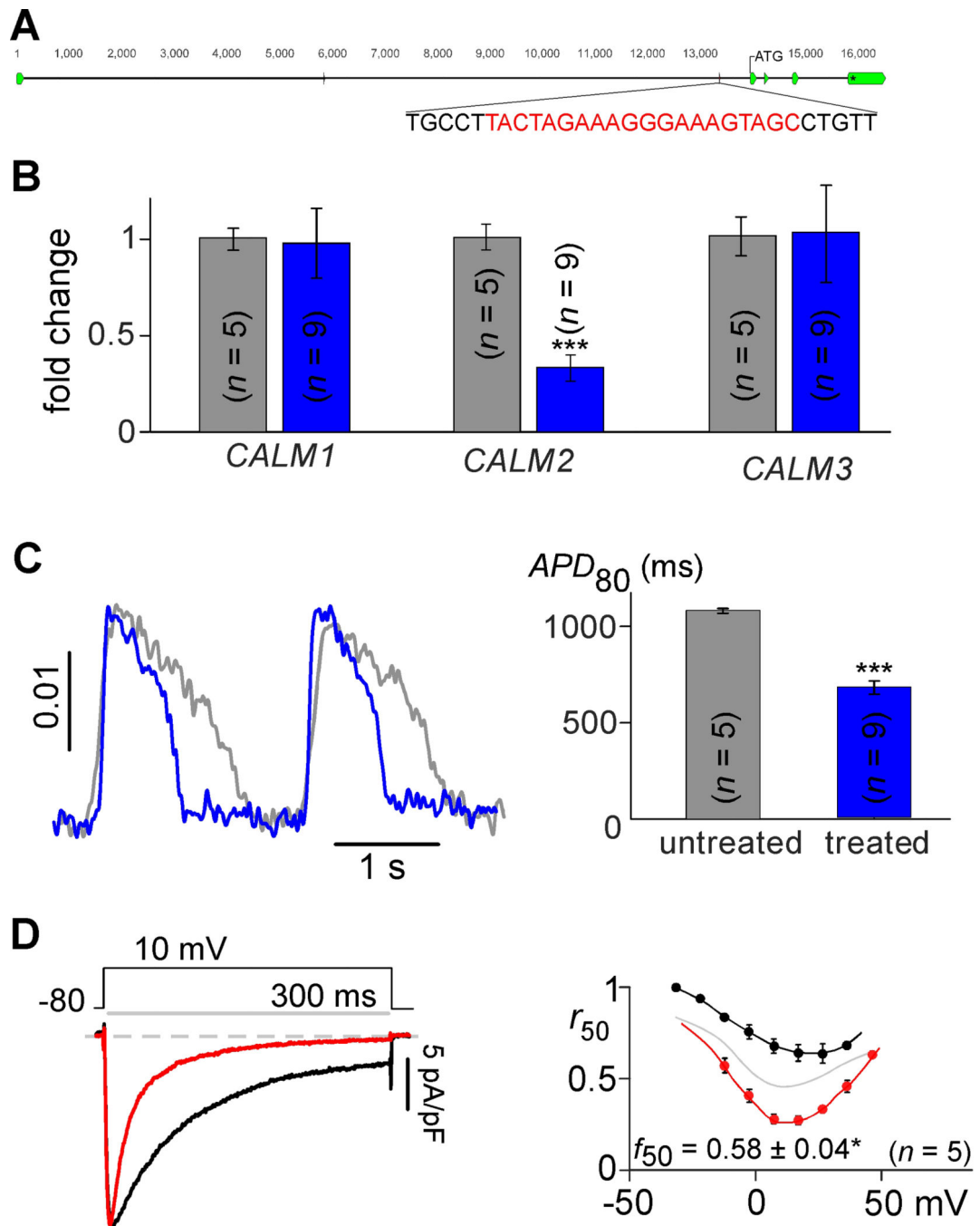


**Figure 4. Functional rescue of calmodulinopathy via CRISPRi treatment**

**A**, The genomic *CALM2* gene showing the location of each exon (green). The gRNA sequence (red) is located in an intron prior to the start codon. **B**, QPCR results indicating mean relative mRNA levels of *CALM1-3* in iPSC<sub>D130G-CaM</sub>-CMs at baseline (gray, n=5) and after CRISPRi treatment (blue, n=9). *CALM2* level is significantly reduced (\*\*\*)  $p < 0.001$  compared to untreated and corrected for unequal variance) with relatively unchanged levels of *CALM1* and *CALM3* expression ( $p > 0.05$ ) following the treatment. Error bars indicate  $\pm$ SEM throughout. **C**, iPSC<sub>D130G-CaM</sub>-CM APs recorded at 0.5-Hz

stimulation using ASAP1 at baseline (gray) and after CRISPRi treatment (blue). Cells correspond to the same monolayers utilized in **B**. APD significantly shortens following CRISPRi treatment (\*\*\*)  $p < 0.001$  compared to untreated, corrected for unequal variance). Scale bar indicates change in fluorescence as measured by  $F/F_0$ . **D**, Exemplar whole cell current recordings in  $\text{Ca}^{2+}$  (red) and  $\text{Ba}^{2+}$  (black) for iPSC<sub>D130G-CaM</sub>-CMs treated with CRISPRi (left panel). Population data demonstrates a return of CDI following treatment for the  $\text{Ca}^{2+}$   $t_{50}$  values (red) as compared to untreated cells (gray, reproduced from Figure 3I). Black shows the  $t_{50}$  values for treated cells in  $\text{Ba}^{2+}$ . (n=5, \*  $p < 0.05$ , compared to untreated, no significant difference in variance between populations). Each biological replicate (n) is an average value of 3 technical replicates/measurements for **B** and **C**. There are no technical replicates in **D**.

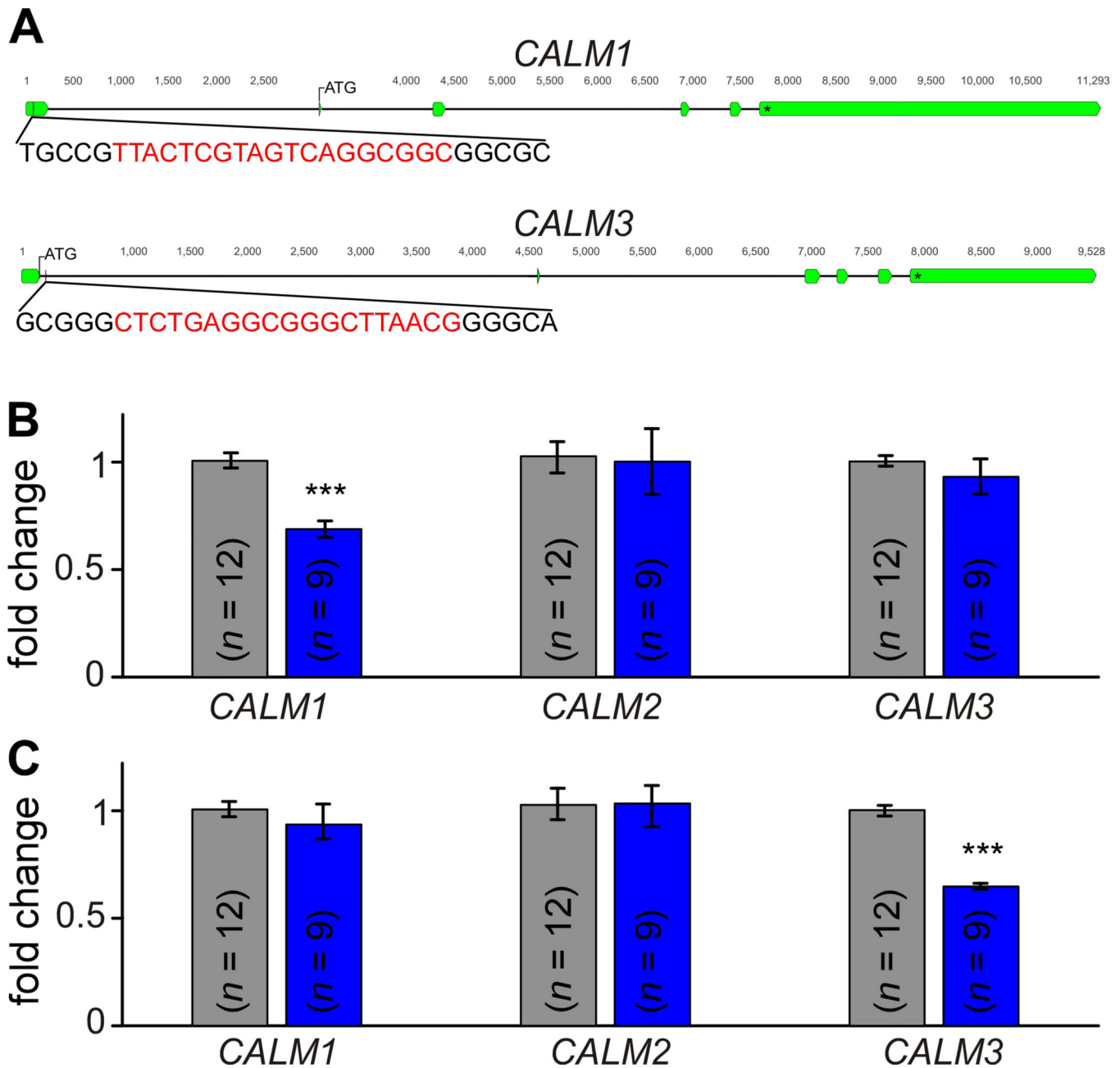


**Figure 5. CRISPRi can also be used to target either *CALM1* or *CALM3***

**A**, The genomic *CALM1* and *CALM3* genes showing location of each exon (green). The gRNA sequence (red) is located in an untranslated exon prior to the start codon of *CALM1*, and in an intron just past the start codon of *CALM3*. **B**, QPCR results indicating mean relative mRNA levels of *CALM1-3* in iPSC<sub>WT</sub>-CMs at baseline (gray, n=12) and after treatment by CRISPRi targeting *CALM1* (blue, n=9). *CALM1* expression is significantly reduced (\*\*\*) p<0.001 compared to untreated, no significant difference in variance between populations) with unaltered levels of *CALM2* and *CALM3* (p>0.05). Error bars indicate  $\pm$ SEM throughout. **C**, QPCR results indicating mean relative mRNA levels of *CALM1-3* in iPSC<sub>WT</sub>-CMs at baseline (gray) and after treatment by CRISPRi targeting *CALM3* (blue,

n=9). *CALM3* expression level is significantly reduced (\*\*\*)  $p < 0.001$  compared to untreated, no significant difference in variance between populations) with unaltered levels of *CALM1* and *CALM2* ( $p > 0.05$ ). Each biological replicate (n) is an average value of 3 technical replicates/measurements.

Author Manuscript

Author Manuscript

Author Manuscript

Author Manuscript